Available online at www.sciencedirect.com
SCIENCE DIRECT
Composites Science and Technology 66 (2006) 1513–1520
COMPOSITES SCIENCE AND TECHNOLOGY
www.elsevier.com/locate/compscitech

Microstructures and wear property of friction stir welded AZ91 Mg/SiC particle reinforced composite

Won-Bae Lee [a], Chang-Yong Lee [a], Myoung-Kyun Kim [b], Jung-Il Yoon [a], Young-Jig Kim [a], Yun-Mo Yoen [c], Seung-Boo Jung [a,*]

[a] Department of Advanced Materials Engineering, Sungkyunkwan University, 300 Cheoncheon-dong, Jangan-gu, Suwon, Kyounggi-do 440-746, Republic of Korea
[b] New Metallic Materials Research Team, RIST, 30 Hyoja-Dong, Nam-gu, Pohang, Kyungbuk, 790-330, Republic of Korea
[c] Department of Automated System, Suwon Science College, Whasung, Kyounggi-do 445-745, Republic of Korea

Received 8 September 2005; received in revised form 21 November 2005; accepted 25 November 2005
Available online 10 January 2006

Abstract

The microstructures and wear property of friction stir welded AZ91 Mg alloy/SiC particle reinforced composite (AZ91/SiC/10p) were investigated. The initial microstructures of the AZ91/SiC/10p were composed of irregularly distributed β-phases ($Al_{12}Mg_{17}$) and agglomerated SiC particles, while the friction stir weld zone was characterized by the homogeneous distribution of SiC particles, the recrystallized grain structure and the dissolution of β-phase. Thank to the microstructural modification, an improvement in the hardness and wear property of the weld zone were observed as compared to those of the base metal. The hardness near the weld zone was a higher and more homogeneously distributed and the wear resistance within the weld zone, as evaluated by the specific wear loss, was superior, as compared with the base metal.

Keywords: A. Particle-reinforced composites; B. Friction/wear; D. Scanning electron microscopy; E. Welding/joining; E. Friction stir welding

1. Introduction

Mg alloys, owing to their low density and high stiffness-to-weight ratio, are gaining increasing importance as a structural material for applications in which weight reduction is critical. However, Mg alloys have not traditionally been used for high performance applications due to their low mechanical properties at room and elevated temperatures. Therefore, particles reinforced Mg-based MMCs have been fabricated by various methods, in an attempt to obtain suitable lightweight materials with better mechanical properties [1–6].

When these composites are practically utilized as the structural components, they often need to be joined to other components made of similar composite or other metallic materials. Therefore, the development of reliable and economic joining techniques is of significant importance in order to assure the successful commercialization of these composites. However, the joining of these composites by conventional fusion welding represents a significant challenge due to the segregation and/or reaction of the reinforcement particles in the fusion zone [7]. The problems encountered during the fusion welding of discontinuously reinforced Al metal matrix composites (MMC) are difficult mixing with the filler materials, the microsegregation or inhomogeneous distribution of the particles and the SiC dissolution resulting in the formation of a large amount of coarse carbide during the melting stage [8–12]. Since the friction stir welding (FSW) process does not fuse the reinforcement particles and matrix materials, these problems can be avoided.

For the FSW of similar Al based MMCs [13–15], the wear of the rotating tool during the FSW and the distribu-

* Corresponding author. Tel.: +82 312907359; fax: +82 312907371.
E-mail address: sbjung@skku.ac.kr (S.-B. Jung).

0266-3538/$ - see front matter © 2005 Elsevier Ltd. All rights reserved.
doi:10.1016/j.compscitech.2005.11.023

tion of the reinforcement particles in the weld zone have been extensively studied. In the case of FSW between the Al base MMC and the monolithic alloy [16], the microstructures of the weld zone were affected by the locations relative to the tool rotating directions and characterized by the eutectic melting, the formation of strings and the fragmentation of the particles. The FSW of Al–Si eutectic alloy resulted in the creation of homogeneously distributed Si particles and an Al matrix with fine recrystallized grain structures in the weld zone [17].

The modified FSW process, namely the friction stir processing (FSP), is increasingly used as a surface modification method, which produce a more homogeneous microstructure and higher mechanical properties [18], and as a grain size refinement technique which leads to superplasticity at high temperature and strain rate in the stirred zone [19]. The FSP is expected to be efficient for the structural materials having a non-homogeneous microstructure and to confer special mechanical properties, especially higher wear resistance, on the stirred surfaces.

In this study, we investigated the microstructures near the FSW zone of AZ91/SiC/10p and considered the effect of the microstructural issues on the hardness distribution and wear properties. Based on the wear resistance, we indirectly evaluated the applicability of the FSP to the surface modification of the AZ91/SiC/10p.

2. Experimental procedure

The material used in this study was 10 vol.% SiC particles reinforced AZ91 Mg alloy, which was fabricated by the Rotation-Cylinder Method (RCM), for which the details of the manufacturing process are available in the literature [20]. For the FSW process, the block shaped specimens were sliced by electro discharge machining (EDM). The dimensions of the specimens were $70 \times 70 \times 4$ (mm). Fig. 1 shows the upper surfaces after FSW of AZ91/SiC/10p with different tool rotation and welding speeds. The welding condition which was a rotation speed of 1250 rpm and a welding speed of 32 mm/min only allowed a smoother upper-surface without surface defect to be generated and was decided to optimum condition in the present study. The tilted angle was 3°.

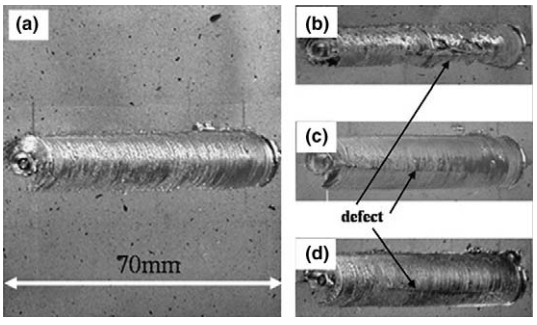

Fig. 1. Upper surface of FSW zone of AZ91/SiCp composite with different FSW conditions: (a) 1250 rpm and 32 mm/min, (b) 2500 rpm and 41 mm/min, (c) 1250 rpm and 41 mm/min and (d) 1250 rpm and 22 mm/min.

The welding tool was rotated in the clock-wise direction, while the specimen, which was attached to the backing plate, was moved. The tool material was SKD 11 (JIS) tool steel with following composition: 1.5%C, 0.4%Si, 0.6%Mn, 0.5%Ni, 12%Cr, 1%Mo, balanced Fe.

The microstructures near the weld zone were examined using optical microscopy (OM) and scanning electron microscopy (SEM). The material was prepared by standard metallographic techniques and etched with a solution which was composed of ethyl alcohol, distilled water, acetic acid and picric acid for 30 s. The phase analysis of the BM and weld zone was carried out with energy dispersive X-ray spectrometer (EDS) and electron probe micro analyzer (EPMA).

The Vickers hardness profile near the weld zone was measured on a cross section perpendicular to the welding direction while applying a 200 g load for 10 s.

The Oghoshi wear testing for the AZ91, AZ91/SiC/10p and the FSW zone of the AZ91/SiC/10p were performed under wet sliding conditions for 1000 s against a rotating austenite cast iron disc (hardness 200 Hv) with a constant load (50 N) and sliding velocity (1 m/s) and dilute water was used as the lubricant. Prior to testing, both the disc and the specimen were ground using 1000 grit SiC paper, and then cleaned in acetone. The measured wear resistance was expressed as the specific wear loss W, according to the following equation:

$$W = Bb^3/8rPl,$$

where B is the thickness of the rotor (3.2 mm), r is the radius of the rotor (20 mm), b is the length of the wear trace, P is the applied load (50 N) and l is the sliding distance (10^3 mm).

3. Results and discussion

Fig. 2 shows the SEM microstructures and EDS phase analysis of the initial AZ91/SiC/10p (Base Metal, BM). The initial AZ91/SiC/10p is composed of four different phases, such as the primary α-Mg phase, the eutectic α-Mg phase with a higher Al content, the eutectic β-phase ($Al_{12}Mg_{17}$) containing 62.32 at% of Mg and 35.04 at% of Al and the SiC particles. The SiC particles are inhomogeneously distributed in the α-Mg matrix, as shown in Fig. 2(c). The size of the SiC particles is approximately 6.5 μm and their shape is polygonal.

Fig. 3 shows the macroimage of the weld zone (a), along with the optical microstructures of the BM (b–d) and each weld zone (e–g). A representative microstructure of the BM is shown in Fig. 3(b), while the segregation of the SiC particles is partially observed, with the existence of a poor-SiC region (c) and a rich-SiC region (d). The microstructure of the BM consists of the darker-colored portion of the SiC phase, the gray-colored portion of the primary α-Mg phase and the lighter-colored portion of the eutectic phase. Fig. 3(e)–(g) represents the heat affected zone (HAZ), the thermo-mechanical affected zone (TMAZ) and the stir zone

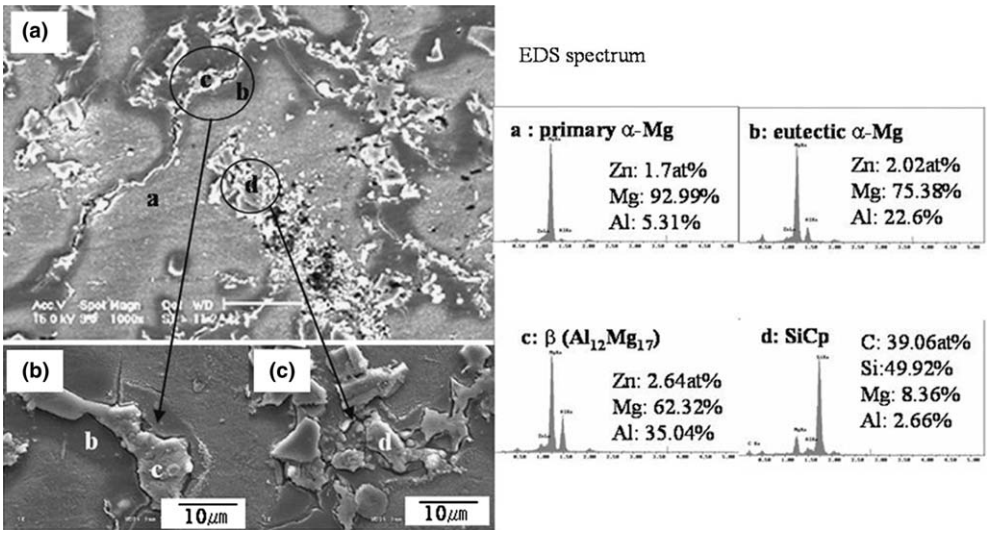

Fig. 2. SEM microstructures and EDS phase analysis of the BM: (a) BM, (b) eutectic α-Mg and β ($Al_{12}Mg_{17}$) and (c) SiCp.

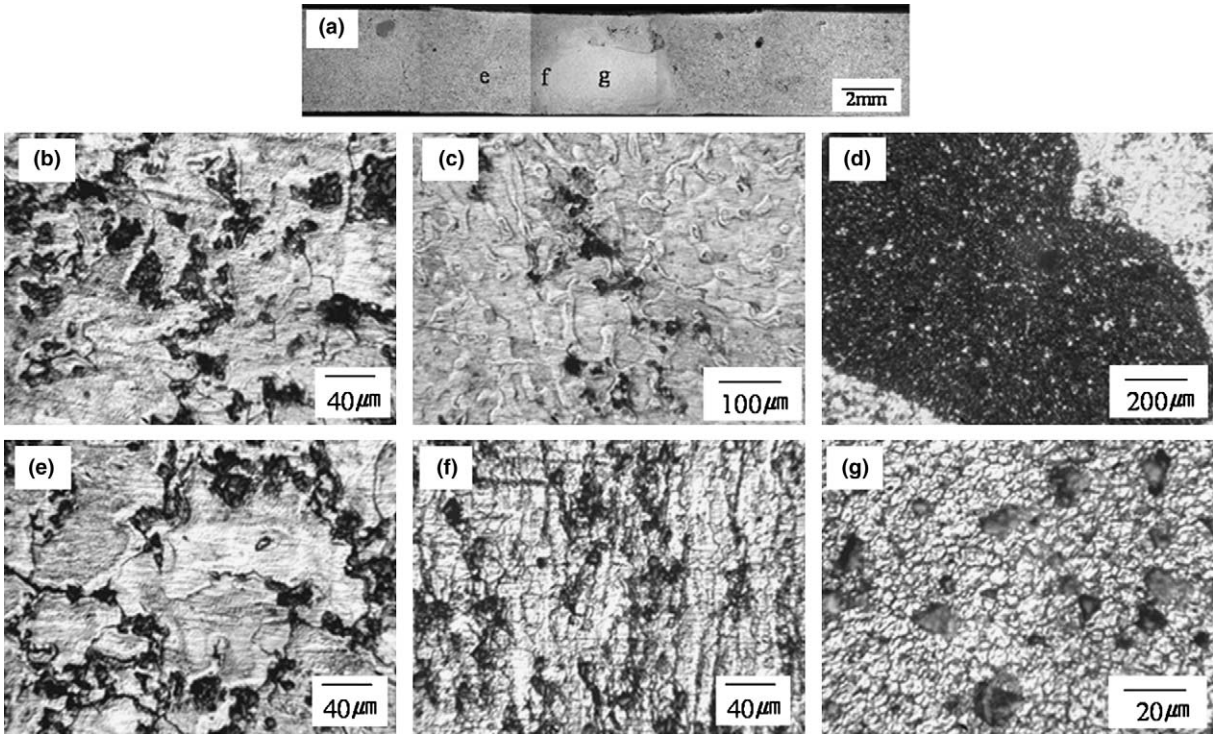

Fig. 3. Macroimage of the weld zone (a); related optical microstructures indicated in the macroimage: (b)–(d) BM; (e) HAZ; (f) TMAZ and (g) SZ.

(SZ), respectively. Region (e) has a similar microstructure to the BM, while showing a slightly lower fraction of the β-phase. The transition region between the SZ and the HAZ are observed in the TMAZ (f). The particles in the TMAZ are continuously aligned in a vertical direction and finely equiaxed grains are observed. Region (g) is characterized by the presence of a recrystallized grain structure and homogeneously distributed particles. The recrystallized grains were equiaxed and have a similar size distribution. Grain structures in the SZ and the TMAZ had fine and equiaxed grains due to the recrystallization, while particles distributions were different because they received a different stirring action. In the case of FSW of Al alloy [21], grain structures in the TMAZ and the SZ were quite different and represented dynamic recovered and recrystallized structure, respectively because high stacking fault energy of Al alloy resulted in the retaining of recovered structure in TMAZ. Mg alloy having hexagonal close packed (HCP) structure can be more easily recrystallized even at the TMAZ, consequently, FSW of Mg alloy resulted in the same recrystallized grain structure in the TMAZ and the SZ [22].

Fig. 4 shows the SEM microstructures of the BM (a), the HAZ (b), the TMAZ (c) and the SZ (d), which represent more detail distribution of the particles. Both the BM and the HAZ retained the eutectic structure and locally agglomerated SiC particles were observed on the whole regions. In the TMAZ, original structure was disrupted and the band structures that were composed of layers with higher and lower density of particles in turn were aligned with special direction. The region adjacent to the HAZ still had eutectic structure, while eutectic structure disappeared in the region next to the SZ. In the SZ, the eutectic structure almost disappeared and particles were homogeneously distributed. In the TMAZ and SZ, the shape of particles was changed and very smaller particles with lighter-color were observed.

In particular, with regard to the behavior of the β-phases, the TMAZ were characterized by a lower fraction of β-phase, while the SZ was characterized by the disappearance of the β-phases, due to the dissolution into the matrix. Each weld zone experienced a different temperature and, consequently, a temperature gradient must have existed through the weld zone. The lower fraction of the β phase in the HAZ and the TMAZ may be due to the ongoing process of dissolution, while the complete dissolution of the β-phases in the SZ was probably observed because the temperature of the SZ exceeded the dissolution temperature of the β-phase in the Mg matrix.

Fig. 5 shows the SEM (BSE, Back Scattered Electron) microstructures and EDS analysis of the SZ. The particles

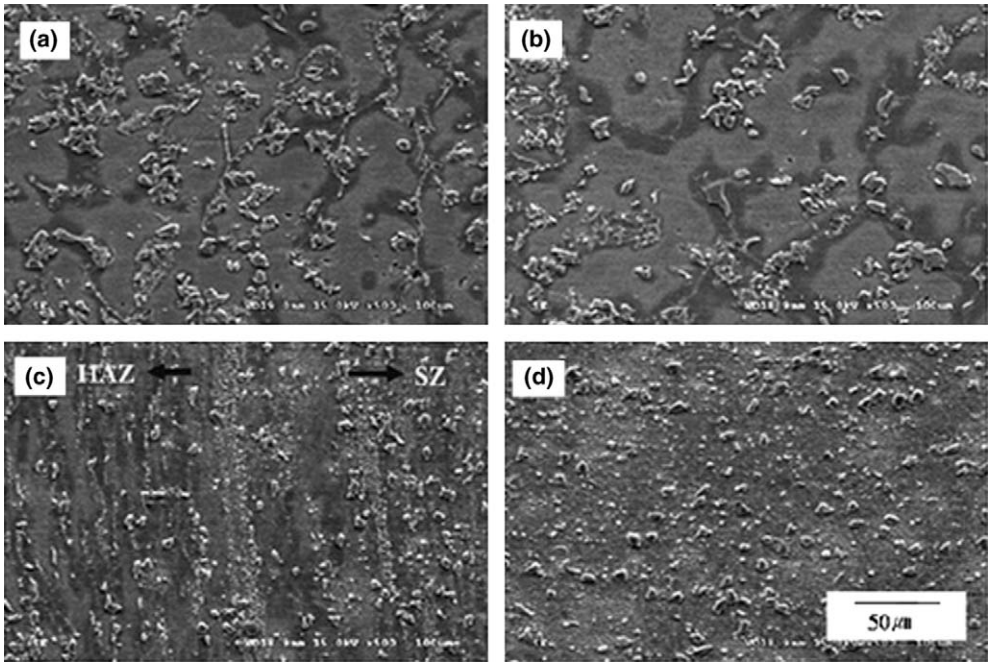

Fig. 4. SEM microstructures of BM (a), HAZ (b), TMAZ (c) and SZ (d).

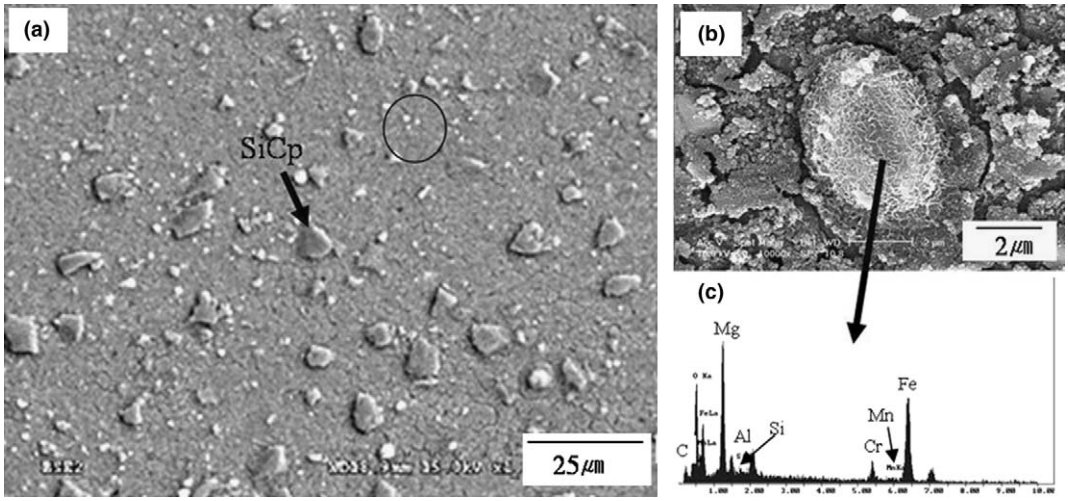

Fig. 5. SEM microstructures and EDS phase analysis of the SZ: (a) overall SZ; (b) phase indicated by circle in (a) and (c) EDS phase analysis of phase b.

presented in the SZ are divided into two types, the darker-colored particles with a diameter of approximately 6 μm and the lighter-colored particles with a diameter of about 1.68 μm. The darker-colored particles were identified as the SiC particles. The phase of the lighter-colored particles cannot be exactly identified by the EDS, because they are composed of many elements, such as Fe, Mg, Al, C, Mn, Cr, Si and O. In particular, the elements, Fe, Cr, Mn and C, might have come from the welding tool. The shape of the SiC particles in the BM was polygonal, while the shape of the SiC particles observed in the SZ had a slightly rounded shape, possibly because the tool stirring had worn the edge of the polygonal SiC particles away. The detection of the elements, Fe, C, Mn, and Cr, in the lighter-colored particles provides evidence of tool wear [13–15].

Fig. 6 shows the EPMA line profile of the interface between dark-colored particles and matrix in the SZ in order to observe microcracks and reaction products. From the Fig. 5, microcracks were observed around the lighter-colored particles. However, microcracks were not detected at the interface between dark-colored particles and matrix judging from the compositional continuity at the interface. The reaction products were not produced at the interface. The FSW of AZ91/SiC/10p can overcome the problem related to the formation of brittle product that brings about serious problem when the fusion welding was applied to join the MMC.

Fig. 7 shows the variation of the SiC particles size with each weld zone and the recrystallized grain size in the TMAZ and the SZ. The average sizes of SiC particles in the BM and the HAZ were approximately 7.5 and 7.3 μm respectively, and were bigger than those of the TMAZ and the SZ. The average sizes of SiC particles in the SZ and the TMAZ were 5.5 and 5.0 μm respectively, and the lighter-colored small particles were only observed in the SZ and the TMAZ. From the standard deviation factor, the distribution of SiC particles in the weld zone was more homogeneous than those of the BM and the HAZ. Locally agglomerated SiC particles with different size and shape were changed into the homogeneously distributed SiC particles with similar size and shape in the TMAZ and the SZ due to tool's stirring action. Recrystallized grains observed in the TMAZ were slightly bigger than those of the SZ, while the size difference of the grains slightly increased. These results mean that recrystallized grains in the SZ showed more homogeneous distribution.

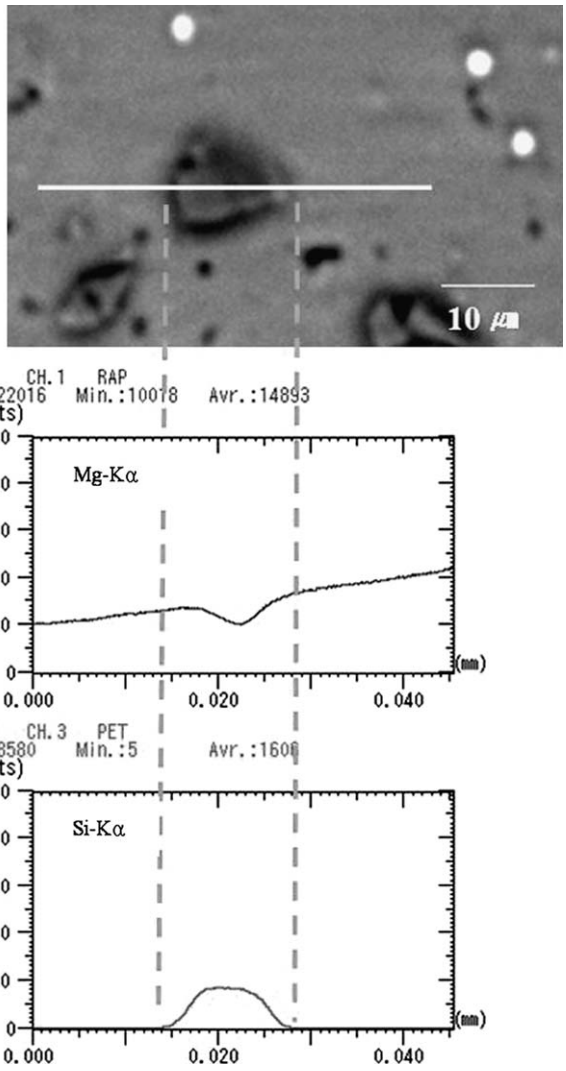

Fig. 6. EMPA line profile of the interface between SiC particle and matrix.

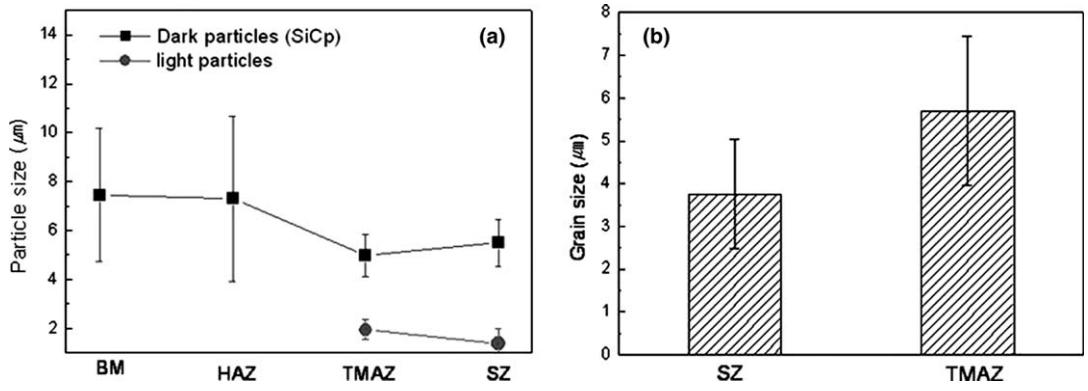

Fig. 7. Variation of the SiC particle (a) and recrystallized grain size (b) with different weld zone.

Fig. 8 shows the hardness distribution near the weld zone measured along with several lines. The transverse hardness distribution (a) was higher hardness in the weld zone than in the BM. The BM shows a non-uniform hardness distribution, ranging from 60 to 80 HV, because the BM is the cast structure consisting of non-homogeneously distributed SiC particles and β intermetallic phases. However, the weld zone shows a higher average hardness of 95HV and only a small fluctuation in the hardness, because the weld zone including the SZ and the TMAZ had a fine recrystallized grain structure and contained homogeneously distributed SiC particles and finely dispersed lighter-colored particles (phase containing Fe, Mg, Al, C, Mn, Cr, Si and O). Within the SZ (b), the hardness of

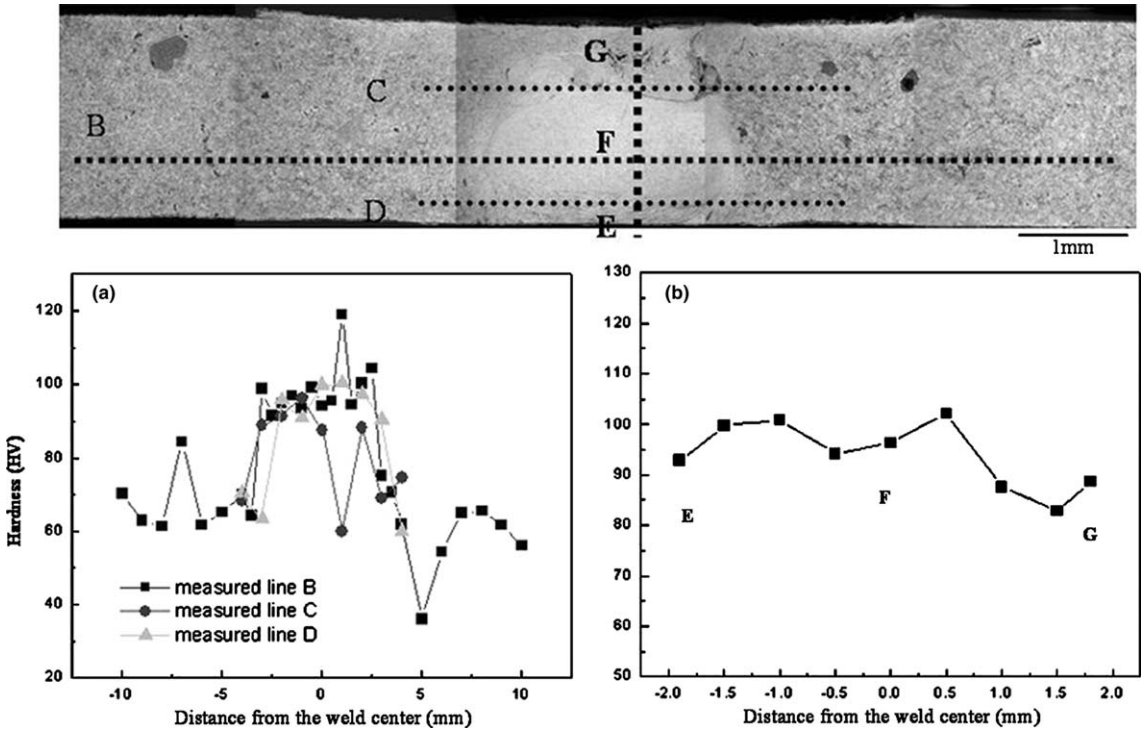

Fig. 8. Hardness distribution near the weld zone: (a) transverse hardness distribution and (b) hardness distribution in SZ from point E to G.

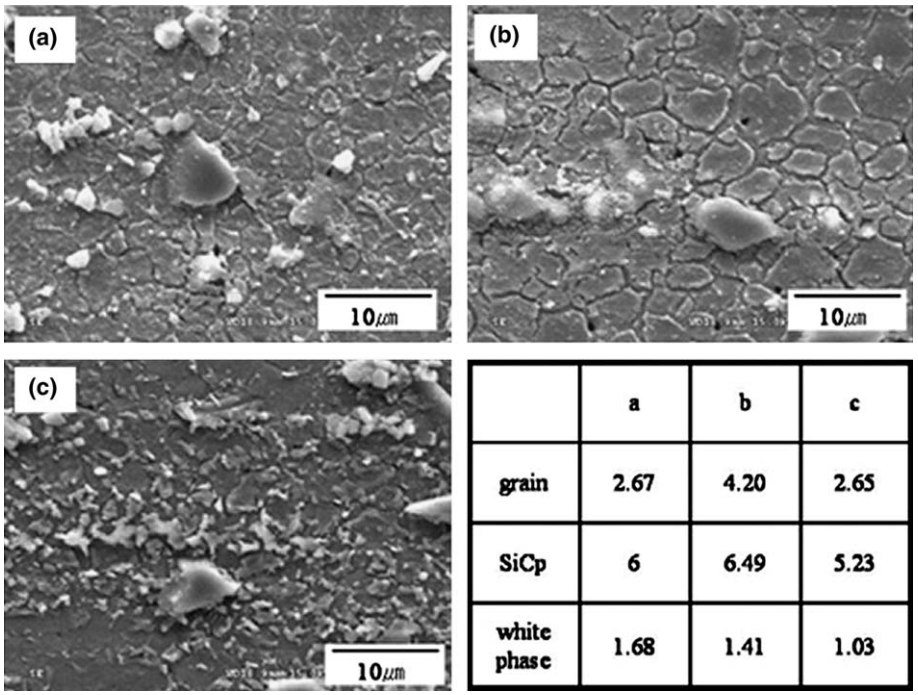

	a	b	c
grain	2.67	4.20	2.65
SiCp	6	6.49	5.23
white phase	1.68	1.41	1.03

Fig. 9. SEM microstructural variation of the each SZ: (a) central SZ, (b) upper SZ, (c) lower SZ and table listing sizes of grains and particles (unit: μm).

the lower SZ (E) is different from that of the upper SZ (G). The upper SZ has a slightly lower hardness than those of the lower and central SZ. The microstructural characteristics, such as the size of the grains, SiC and lighter-colored particles, which can affect the mechanical properties, are listed in Fig. 9. The sizes of the particles (SiC and lighter-colored phase) are not remarkably different, while the mean recrystallized grain size of the upper SZ is quite different from that of the central and lower SZ. Although other factors, such as the grain texture, the grain boundary orientation and the dislocation density, might affect the hardness distribution, the presence of coarsened recrystallized grains was mainly attributed to the lower hardness of the upper SZ. Each region of the SZ was subjected to different a thermomechanical effects, due to the shape of the welding tool. In particular, the upper SZ was in direct contact with the shoulder of the rotating welding tool, due to the tilting of the welding tool. Therefore, this region might have attained a higher temperature than those of the central and lower SZ and this higher temperature would have accelerated the grain growth after the FSW in the upper SZ.

Fig. 10 shows the specific wear loss (mm^2/Nm) values and the worn surfaces of the AZ91 (a), the AZ91/SiC/10p (b) and the FSW zone of the AZ91/SiC/10p (c). The specific wear loss values are approximately 5.5 (a), 2.1 (b) and 1.6 mm^2/Nm (c), respectively. These results mean that the wear resistance was remarkably improved by the addition of the SiC particles to the AZ91 Mg alloys and the friction stirring also helped to improve the wear properties in the stirred zone of the AZ91/SiC/10p.

Fig. 11 shows the SEM micrographs of the worn surfaces of the AZ91 (a), the AZ91/SiC/10p (b) and the FSW zone of the AZ91/SiC/10p (c). In the case of the AZ91 (a), the worn surface was composed of the Mg matrix and the $Al_{12}Mg_{17}$ intermetallic compound, and, the straight wear traces were observed over the whole the Mg matrix and intermetallic part. The existence of the straight wear traces in the $Al_{12}Mg_{17}$ intermetallic compound means that these brittle and coarse $Al_{12}Mg_{17}$ intermetallic compounds did not effectively act as an obstacle to the wear by the sliding count part materials. In the case of the AZ91/SiC/10p (b), the worn surface was composed of the Mg matrix, the $Al_{12}Mg_{17}$ and the partially segregated SiC particles, and the wear traces still remained straight, although, non-straight wear traces were also observed in localized regions. The distances between each wear traces became wider. The existence of non-straight wear trace and wider distance between each wear traces mean that

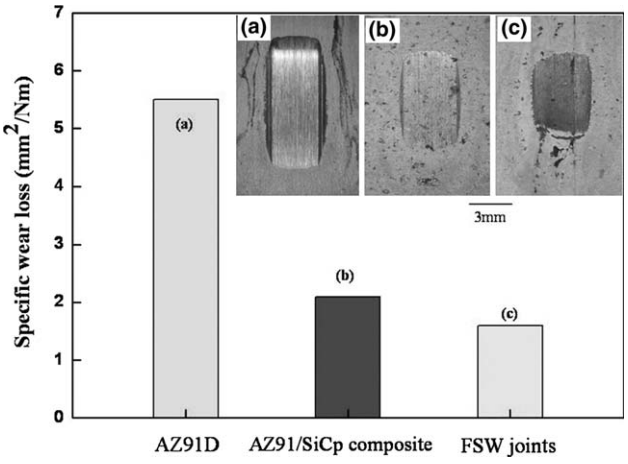

Fig. 10. Variation of the specific wear loss and the worn surfaces for the AZ91 (a), the AZ91/SiCp composite (b) and the FSW zone of the AZ91/SiCp composite.

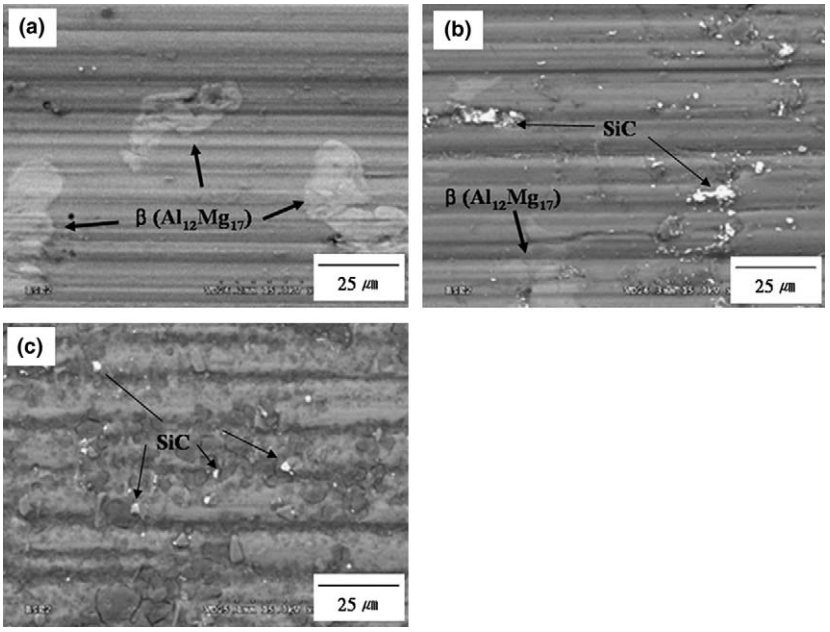

Fig. 11. SEM micrographs of the worn surface for the AZ91 (a), the AZ91/SiCp composite (b) and the FSW zone of the AZ91/SiCp composite.

distributed SiC particles acted as a barrier to the wear. In the worn surface of the FSW zone of AZ91/SiC/10p (c), the distance between the wear traces was wider and the wear traces were bent and their paths unclear. The equiaxed grains and homogeneously distributed SiC particles located in the equiaxed grain boundaries positively affected the wear resistance. The friction stirring effects on the weld zone of the AZ91/SiC/10p led to the development of homogeneous microstructures and higher mechanical properties such as improved hardness and wear resistance. Based on the above results, it can be concluded that the FSP can be used to modify the surface properties of the materials having poorly homogeneous microstructures. Result about FSP of AZ91/SiC/10p as surface modification method will be followed in the future paper.

4. Summary

The FSW of AZ91/SiC/10p resulted in the production of homogeneously distributed SiC particles, the dissolution of the β-phase, the formation of lighter-colored phases containing elements from the welding tool and a finely recrystallized grain structure in the weld zone. The formation of phases containing elements originating from the welding tool provides evidence of the abrasion of the welding tool during the friction stir welding. The hardness of the weld zone was homogeneous and showed higher values than that of the BM and the wear property was also improved in the weld zone.

References

[1] Lianxi H, Erde W. Fabrication and mechanical properties of SiCw/ZK51A magnesium matrix composite by two-step squeeze casting. Mater Sci Eng A 2000;278:267–71.
[2] Wang AH, Yue TM. YAG laser cladding of an Al–Si alloy onto an Mg/SiC composite for the improvement of corrosion resistance. Compos Sci Technol 2001;61:1549–54.
[3] Lim CYH, Lim SC, Gupta M. Wear behaviour of SiC_p-reinforced magnesium matrix composites. Wear 2003;255:629–37.
[4] Kumar S, Ingole S, Dieringa H, Kainer K-U. Analysis of thermal cycling curves of short fibre reinforced Mg-MMCs. Compos Sci Technol 2003;63:1805–14.
[5] El-Saeid Essa Y, Perez-Castellanos JL. Effect of the strain rate and temperature on the mechanical behaviour of a Mg–5%Zn alloy reinforced with SiC particles. J Mater Process Tech 2003;143(144):856–9.
[6] Dong Q, Chen LQ, Zhao MJ, Bi J. Synthesis of TiCp reinforced magnesium matrix composites by in situ reactive infiltration process. Mater Lett 2004;58:920–6.
[7] Cavaliere P, Cerri E, Marzoli L, Dos Santos J. Friction stir welding of ceramic particle reinforced aluminum based metal matrix composite. Appl Compos Mater 2004;11:247–58.
[8] Zhang XP, Quan GF, Wei W. Preliminary investigation on joining performance of SiC_p-reinforced aluminium metal matrix composite (Al/SiC_p–MMC) by vacuum brazing. Compos Part A—Appl S 1999;30:823–7.
[9] Gomez De Salaza JM, Marrena MI. Dissimilar fusion welding of AA7020/MMC reinforced with Al_2O_3 particles. Mater Sci Eng A 2003;352:162–8.
[10] Wang HM, Chen YL, Yu LG. In-situ' weld-alloying/laser beam welding of SiCp/6061Al MMC. Mater Sci Eng A 2001;293:1–6.
[11] Urena A, Escalera MD, Gil L. Influence of interface reactions on fracture mechanisms in TIG arc-welded aluminium matrix composites. Compos Sci Technol 2000;60:613–22.
[12] Lee CS, Li H, Chandel RS. Vacuum-free diffusion bonding of aluminium metal matrix composite. J Mater Process Tech 1999;89(90):326–30.
[13] Shindo DJ, Rivera AR, Murr LE. Shape optimization for tool wear in the friction-stir welding of cast Al 359–20%SiC MMC. J Mater Sci 2002;37:4999–5005.
[14] Prado RA, Murr LE, Soto KF, McClure JC. Self-optimization in tool wear for friction-stir welding of Al 6061 + 20% Al_2O_3 MMC. Mater Sci Eng A 2002;349:156–65.
[15] Prado RA, Murr LE, Shindo DJ, Soto KF. Tool wear in the friction-stir welding of aluminum alloy 6061 + 20% Al_2O_3: a preliminary study. Scripta Mater 2001;45:75–80.
[16] Wert JA. Microstructures of friction stir weld joints between an aluminium–base metal matrix composite and a monolithic aluminium alloy. Scripta Mater 2003;49:607–12.
[17] Lee WB, Yeon YM, Jung SB. The improvement of mechanical properties of friction-stir-welded A356 Al alloy. Mater Sci Eng A 2003;355:154–9.
[18] Mishra RS, Ma ZY, Charit I. Friction stir processing: a novel technique for fabrication of surface composite. Mater Sci Eng A 2003;341:307–10.
[19] Charit I, Mishra RS. High strain rate superplasticity in a commercial 2024 Al alloy via friction stir processing. Mater Sci Eng A 2003;359:290–6.
[20] Kim SK, Kim YJ. Rotation-cylinder method for fabrication of SiC particulate reinforced magnesium composites. Met Mater-Int 2000;6:359–64.
[21] Su J-Q, Nelson TW, Mishra R, Mahoney M. Microstructural investigation of friction stir welded 7050-T651 aluminium. Acta Mater 2003;51(3):713–29.
[22] Lee WB, Yeon YM, Jung SB. Joint properties of friction stir welded AZ31B-H24 magnesium alloy. Mater Sci Technol 2003;19:785–90.